Gasification of Graphite and Coke in Carbon–Carbon Dioxide–Sodium or Potassium Carbonate Systems

ARTICLE · APRIL 2014

DOI: 10.1021/ie4039955

5 AUTHORS, INCLUDING:

Kejiang Li
University of Toronto
16 PUBLICATIONS **23** CITATIONS
SEE PROFILE

Jianliang Zhang
University of Science and Technology Beijing
25 PUBLICATIONS **50** CITATIONS
SEE PROFILE

I&EC research
Industrial & Engineering Chemistry Research

Article

pubs.acs.org/IECR

Gasification of Graphite and Coke in Carbon–Carbon Dioxide–Sodium or Potassium Carbonate Systems

Kejiang Li,[†,‡] Jianliang Zhang,*[,†,‡] Zhengjian Liu,[†,‡] Xiaojun Ning,[†,‡] and Tianqiu Wang[§]

[†]School of Metallurgical and Ecological Engineering and [‡]State Key Laboratory of Advanced Metallurgy, University of Science and Technology Beijing, Beijing 100083, China

[§]Iron Making Branch, Baoshan Iron & Steel Co Ltd., Shanghai, 200941, China

ABSTRACT: The thermodynamics of possible reactions, including gasification and reduction reactions, in carbon–carbon dioxide–sodium or potassium carbonate systems was analyzed first. And then, the gasification reactions of graphite and coke with CO_2 in this system were studied kinetically by temperature programmed thermogravimetry. The results showed that the carbon conversion curve shifted to a lower temperature zone after Na_2CO_3 or K_2CO_3 was added, and graphite was more susceptible than coke to be catalyzed by Na_2CO_3 or K_2CO_3. Ten kinetic equations were adopted to simulate the reaction process using the method of Coats–Redfern. The Avrami–Erofeev equation was found to be the most probable kinetic equation, with which the values of activation energy and frequency factor were calculated. The kinetic simulation indicated that the activation energy of coke carbon had been activated to the lowest level by its inner factors, thus it was difficult to be reduced by adding Na_2CO_3 or K_2CO_3. The kinetic compensation effect was confirmed to exist in both graphite gasification and coke gasification. X-ray diffraction and Raman spectra were used to characterize the inner difference between graphite and coke, which showed that coke carbon structure was greatly different from graphite structure because of its highly disordered and heterogeneous carbon structure.

1. INTRODUCTION

The high energy consumption and high emission of blast furnace ironmaking have gone against with the low carbon and environmental protection strategy in many countries, which have caused great pressure and challenge to blast furnace ironmaking.[1,2] The control and adjustment of chemical reactions in blast furnace have become the main measures to improve the utilization efficiency of energy from fuels, especially coke which is the main resource of carbon and energy in blast furnace.[3] The process parameters of coke (carbon) gasification reaction, especially the initial reaction temperature (T_0), final reaction temperature (T_f), and the temperature where the reaction rate reaches the peak (T_{max}), have a great influence on the reduction process of iron ore and the temperature distribution in blast furnace.[4] The gasification reaction of coke with CO_2 occurs mainly in two regions. (i) In the raceway: coke carbon reacts with CO_2 produced by the combustion of carbon with O_2 in this region. (ii) In the lower part of blast furnace where temperature is above 1000 °C: CO_2 originated from the indirect reduction of iron oxide by CO reacts with coke carbon to produce CO again. The coke gasification with CO_2 produces a steady flow of CO gas to reduce the iron oxide and other minerals in blast furnace. This reaction is a strong endothermic reaction. Thus, coke plays important roles in both providing the reducing gas and cooling the gas from the combustion zone in the blast furnace. These roles are achieved by the coke (carbon) gasification and will affect the process of reduction and heat exchange. In addition, the gasification of coke with CO_2 is one of the most important factors that influence the coke fine generation and stability of burden structure in blast furnace.[5,6]

The reactivity of coke with CO_2 is mainly governed by two classes of factors. One is the structure of coke, including the coke carbon structure, pore structure, etc.[7,8] The other is the catalytic effect of minerals from both inside and outside of coke.[5] In recent years, the influence of minerals, especially alkalis, on coke carbon reactivity has gained much attention.[9,10] A certain amount of alkalis will enter the blast furnace along with the burden materials. As alkalis cannot be effectively discharged from the blast furnace, a cycle of continuous enrichment is brought by the remaining alkalis in different forms in different regions of the blast furnace.[11] Both theoretical calculation[11] and investigation of coke samples from dissected blast furnace[12] have confirmed that alkali in the middle and upper part of blast furnace is in the form of alkali carbonates. As alkali carbonates have been confirmed to have catalytic influence on the carbon gasification with CO_2,[13−15] the theory of catalytic effect on carbon gasification is usually applied to explain that on coke gasification. However, the structure of coke is dramatically different from that of pure carbon, such as highly ordered graphite.[16] Thus, coke gasification and graphite gasification may be influenced in different ways and degrees by alkali carbonates with different mechanisms.

Considering graphite crystal have been confirmed in blast furnace coke and the degree of graphitization increases with the increase of temperature in blast furnace,[6,17] graphite and coke were chosen to conduct a series of comparative experiments in this study. Thermogravimetric analysis (TGA) was used to

Received: November 26, 2013
Accepted: March 17, 2014
Published: March 17, 2014

dx.doi.org/10.1021/ie4039955 | *Ind. Eng. Chem. Res.* 2014, 53, 5737−5748

investigate the graphite gasification and coke gasification with CO_2 under the influence of alkali carbonates. The gasification reactions of carbon (graphite) with CO_2 was analyzed first using FactSage to ensure that the experimental scheme met the thermodynamic conditions. The reduction reactions of Na_2CO_3 and K_2CO_3 were also calculated by FactSage to demonstrate that those reactions would not happen before their catalytic effect started to work. The characteristic temperatures of gasification reactions of both graphite and coke with CO_2 were tested with thermogravity (TG) to compare the difference between graphite gasification and coke gasification under the influence of Na_2CO_3 or K_2CO_3. Ten kinetic models were adopted and calculated to determine the most probable mechanism function for the gasification process. The kinetic parameters were obtained based on the most probable kinetic mechanism function. Kinetic analysis indicated that graphite and coke had different inner factors which determined its reaction procedure with CO_2. To investigate the inner difference between graphite and coke, the samples were tested by X-ray diffraction, and a laser with a wavelength of 532 nm was used to acquire the Raman spectra of graphite and coke. In addition to the D and G bands, carefully assigned Raman bands based on the chemical structural features of carbon structure were used to curve-fit the Raman spectra.

2. MATERIALS AND METHODS

2.1. Raw Material. In this study, all the chemical reagent powder, including graphite (purity ≥99.85%), Na_2CO_3 (purity ≥99.8%), and K_2CO_3 (purity ≥99.0%) were obtained from Sinopharm Chemical Regent Co., Ltd. The coke sample was obtained from a large sized (4000 m^3) blast furnace (no. 4) of Baosteel at Baoshan, Shanghai. Proximate and ultimate analysis of coke was made first and the results are shown in Table 1.

Table 1. Proximate and Ultimate Analysis of Coke

Proximate Analysis (wt %, Air Dry Basis)			
moisture	ash yield	volatile matter	fixed carbon
0.20	12.07	1.54	86.19
Ultimate Elemental Analyses (wt %, Air Dry Basis)			
C	H	N	O
85.68	0.18	0.96	0.27

Table 2 shows the elements of inorganic matter of coke, which are represented as oxides. The inorganic matter of coke was mainly comprised of four elements, silicon, aluminum, iron, and calcium with small amounts of titanium, alkalis, and alkaline earths as well as sulfur and phosphorus. The coke was crushed to be similar to graphite in size and surface area before experiment. Figure 1 shows the particle size distribution of graphite powder and coke fine. The specific surface area of graphite and coke were 1.553 and 1.193 $m^2 \cdot cm^{-3}$, which showed both had a similar contact area with gas in the gasification process.

Minerals influenced reactions of coke with gas, metal, and mineral matter, even though their ratios in total coke matter were typically less than 15 wt %.[10,18] The experimental schemes

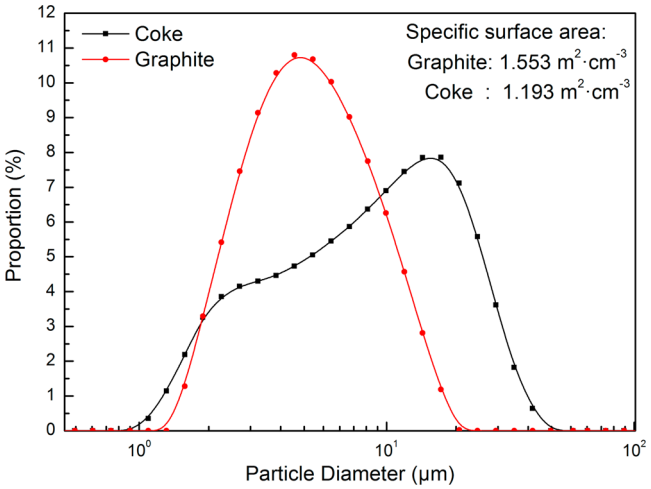

Figure 1. Particle size distribution of coke and graphite.

Table 3. Experimental Scheme for the Mixing of Alkali Carbonates with Graphite and Coke

first group	scheme	second group	scheme
G	100% graphite	C	100% coke
G-K1	0.5% K_2CO_3 + 99.5% graphite	C-K1	0.5% K_2CO_3 + 99.5% coke
G-K2	2.5% K_2CO_3 + 97.5% graphite	C-K2	2.5% K_2CO_3 + 97.5% coke
G-K3	5.0% K_2CO_3+ 95% graphite	C-K3	5.0% K_2CO_3+ 95% coke
G-N1	0.5% Na_2CO_3+ 99.5% graphite	C-N1	0.5% Na_2CO_3+ 99.5% coke
G-N2	2.5% Na_2CO_3+ 97.5% graphite	C-N2	2.5% Na_2CO_3+ 97.5% coke
G-N3	5.0% Na_2CO_3+ 95% graphite	C-N3	5.0% Na_2CO_3+ 95% coke

are shown in Table 3. Two groups of experiments were designed. The first group was based on graphite with 0.0%, 0.5%, 2.5%, and 5.0% Na_2CO_3 or K_2CO_3 added. The second group was based on coke with the same proportions of alkali carbonates added as that of graphite. The mixing materials were blended in agate mortar for 30 min to ensure the mixing homogeneity.

2.2. Apparatus and Procedure. The experiments were conducted using microcomputer differential thermal balance HCT, as shown in Figure 2, produced by Beijing Henven Scientific Instrument Factory. The gasification of the samples was performed in the furnace of the thermobalance under controlled temperature and heating rate to obtain the corresponding thermogravimetry (TG) and differential thermogravimetry (DTG) gasification curves. The TG baselines were corrected by subtraction of predetermined baselines which were determined under identical condition except for the absence of a sample. The heating rate was set at 5 °C/min to eliminate the influence of heat transfer which may cause a thermal gradient in the samples.[19] The sample in the furnace was heated up from ambient temperature to 1200 °C with the

Table 2. Ash Constituent Analysis, Elements as Oxides (wt %)

SiO_2	Al_2O_3	Fe_2O_3	CaO	TiO_2	MgO	Na_2O	K_2O	SO_3	P_2O_5	toal
43.63	31.65	5.29	4.79	1.45	1.09	0.13	0.33	10.98	0.67	100.00

dx.doi.org/10.1021/ie4039955 | Ind. Eng. Chem. Res. 2014, 53, 5737−5748

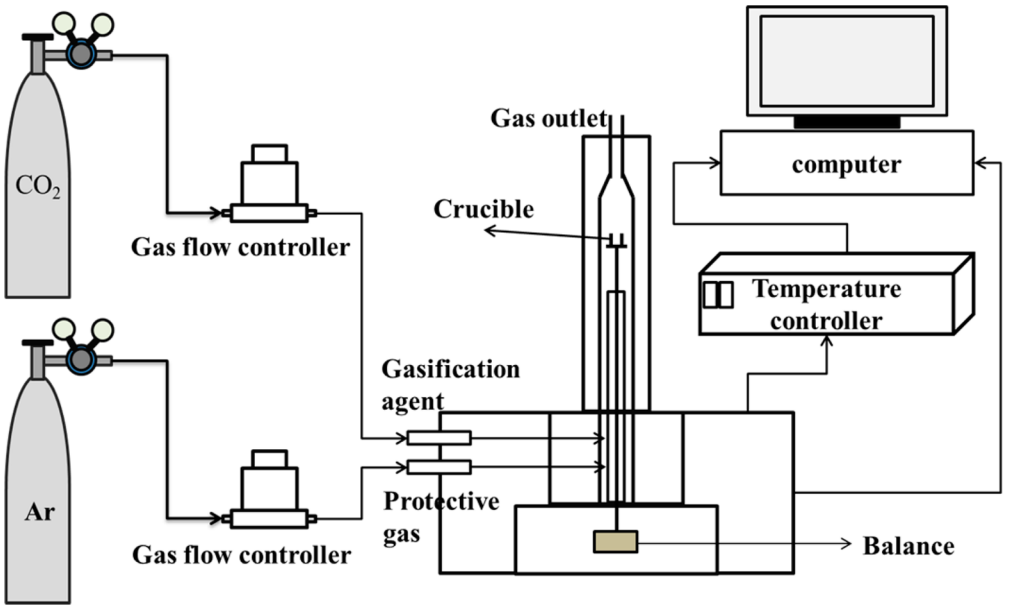

Figure 2. Schematic of the experimental apparatus.

chosen heating rate. In order to eliminate the effects caused by the mass and heat transfer limitations, a small quantity of samples (5 mg) were loaded into an Al_2O_3 crucible for each run under nonisothermal conditions. In addition, oxidizing atmosphere inside the furnace of thermogravimetric analyzer during temperature-programmed gasification was provided by means of a continuous gasflow of 60 mL/min CO_2 (purity ≥99.5%). For each sample and experimental conditions, three repetitive TG curves were obtained to ensure reproducibility of the results.

3. THERMODYNAMIC AND KINETIC ANALYSIS

3.1. Thermodynamic Analysis. The main reaction in this study is carbon gasification, which can be written as follows in general:

$$C + CO_2 = 2CO \tag{1}$$

The Gibbs free energy of chemical reaction can be calculated by subtracting the Gibbs free energy of formation of products from that of reactants. The calculation formula is shown as below:

$$\begin{aligned}\Delta G_r(T) &= 2\Delta_f G_{CO}(T) - \Delta_f G_{CO_2}(T)\\ &= RT \ln K_r\\ &= RT \ln \frac{(P_{CO}/P^{\theta})^2}{P_{CO_2}/P^{\theta}}\end{aligned} \tag{2}$$

Where T (K) is the absolute temperature, $\Delta G_r(T)$ (kJ·mol^{-1}) is the variation of Gibbs free energy between the reactants and products; $\Delta_f G_{CO}(T)$ (kJ·mol^{-1}) is the Gibbs free energy of formation of CO at temperature T, $\Delta_f G_{CO_2}(T)$ (kJ·mol^{-1}) is the Gibbs free energy of formation of CO_2 at temperature T, K_r is the standard equilibrium constant, P_{CO} (Pa) is the equilibrium partial pressure of CO at temperature T, P_{CO_2} (Pa) is the equilibrium partial pressure of CO_2 at temperature T, P^{θ} (atm) is the standard atmospheric pressure. Among the above parameters, $\Delta_f G_{CO}(T)$ and $\Delta_f G_{CO_2}(T)$ could be obtained from the FactSage database. $\Delta G_r(T)$ of the total reaction could be calculated by FactSage.

The relationship of P_{CO} and P_{CO_2} under different pressures can be described as follows.

$$P_{CO_2} + P_{CO} = P \tag{3}$$

$$X_{CO} = 1 - X_{CO_2} \tag{4}$$

Where P (atm) is the pressure of mixing gas of CO_2 and CO, X_{CO} and X_{CO_2} is the mole fraction of CO and CO_2, respectively.

The equilibrium constant based on mole fraction was defined as below.

$$K_x = \frac{(1 - X_{CO_2})^2}{X_{CO_2}} \tag{5}$$

The equilibrium constant based on partial pressure was defined as below.

$$\begin{aligned}K_P &= \frac{(P(1 - X_{CO_2})/P^{\theta})^2}{PX_{CO_2}/P^{\theta}} = \frac{P}{P^{\theta}}\frac{(1 - X_{CO_2})^2}{X_{CO_2}} = \frac{P}{P^{\theta}}K_x\\ &= K_r\end{aligned} \tag{6}$$

According to eq 5, the mole fraction of CO_2 can be calculated as below.

$$X_{CO_2} = \left(\frac{K_x}{2} + 1\right) - \sqrt{\left[\left(\frac{K_x}{2} + 1\right) - 1\right]} \tag{7}$$

Inserting eq 6 into eq 7, the mole fraction of CO_2 can be calculated with the pressure of mixing gas and standard equilibrium constant which can be calculated with eq 2, as expressed in the following form.

$$X_{CO_2} = \left(\frac{K_r/(P/P^{\theta})}{2} + 1\right) - \sqrt{\left[\left(\frac{K_r/(P/P^{\theta})}{2} + 1\right) - 1\right]} \tag{8}$$

dx.doi.org/10.1021/ie4039955 | Ind. Eng. Chem. Res. 2014, 53, 5737−5748

Using eq 4 the mole fraction of CO can be calculated. Thus the gas compositions of equilibrium carbon gasification (eq 1) can be calculated under different temperatures and pressures. The results are shown in Figure 3.

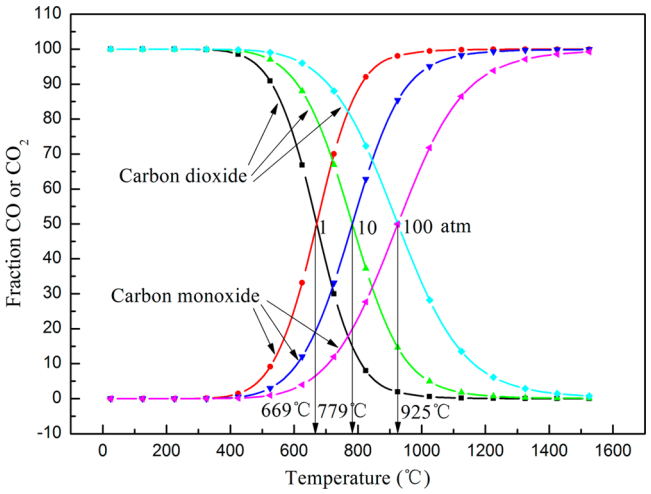

Figure 3. Gas compositions of equilibrium carbon gasification under different temperatures and pressures.

The result of equilibrium calculation shows that the proportion of CO increases with increasing temperature at constant pressure. However, there is an inverse relationship between the fraction of CO and mixing gas pressure at constant temperature. With increasing pressure, the fraction curve of CO shifts to a higher temperature zone, which indicates the high pressure makes it harder for the carbon gasification. At the same temperature, the higher the pressure, the lower the fraction of CO. There is a cross point between the fraction curve of CO and CO_2. The temperature at this point can be defined as the cross temperature between CO and CO_2. The fraction of CO is greater than that of CO_2 when temperature is above the cross temperature, which indicates that less CO_2 can coexist with carbon under equilibrium state. The lower the cross temperature, the easier the carbon gasification. With increasing pressure, the cross temperature increases.

Besides the carbon gasification reaction, the reduction reaction of alkali carbonates by carbon or CO should be considered to make sure they would not happen or affect the carbon gasification. The possible reactions are shown as follows.

$$K_2CO_3 + 2C = 2K + 3CO \quad (9)$$

$$Na_2CO_3 + 2C = 2Na + 3CO \quad (10)$$

$$Na_2CO_3 + CO = 2Na + 2CO_2 \quad (11)$$

$$K_2CO_3 + CO = 2K + 2CO_2 \quad (12)$$

With commercial software FactSage, the Gibbs energy of the above possible reactions was calculated at different temperatures. The results are shown in Figure 4. It can be observed that, the reduction reactions of Na_2CO_3 or K_2CO_3 by CO are impossible when temperature is less than 1130 °C because the ΔG of both reduction reactions is greater than zero within this temperature range. The ΔG of carbon reduction reactions of Na_2CO_3 or K_2CO_3 get lower than zero at 1160 and 1130 °C, respectively, which indicates that those reactions may happen when temperature is greater than 1160 or 1130 °C. However,

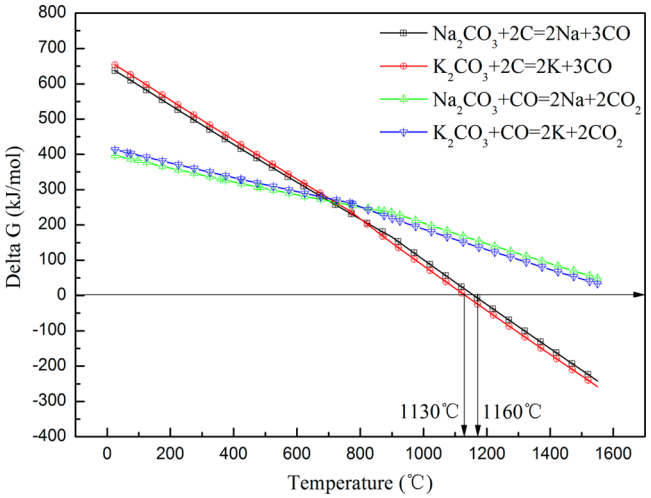

Figure 4. Change of Gibbs energy of possible reduction reactions of alkali carbonates at different temperatures.

as the highest temperature in the present study is 1200 °C, the degree of carbon reduction of Na_2CO_3 and K_2CO_3 is weak enough to be ignorable.

3.2. Kinetics Analysis. *(1) Kinetics Model.* Thermogravimetric analysis (TGA) has been widely used to measure the mass loss as a function of time and temperature to determine kinetic parameters.[20−23] Generally, there are two methods, the isothermal techniques and the nonisothermal studies. The nonisothermal method was adopted to get a mass (or conversion) versus time curve using the TGA in this research. In the present experiments, the mass loss was only caused by the carbon gasification with CO_2, which was shown in eq 1. The carbon conversion (x) can be defined as the ratio of the gasified carbon (graphite or coke) at any time t to the initial carbon (graphite or coke), which was shown as below.

$$x = \frac{m_i - m_t}{m_i - m_f} \quad (13)$$

Where, m_i (mg) is the initial dry sample weight at 800 °C, m_t(mg) is the sample weight at reaction time t, and m_f (mg) is the mass of the sample at the end of the reaction.

As for heterogeneous solid-state reactions, the rate of reaction or conversion, dx/dt, is the function of a temperature and pressure dependent rate constant, $k(T, P_{CO_2})$, and a temperature independent mechanism function of conversion, $f(x)$. The equation can be expressed as follows.

$$\frac{dx}{dt} = k(T, P_{CO_2})f(x) \quad (14)$$

Where, x is the degree of conversion, t (s) is time, and T (K) is thermodynamic temperature.

In this experiment, the partial pressure of CO_2 remains constant during reaction, thus $k(T)$ can be described by the famous Arrhenius equation:

$$k(T) = A \exp\left(-\frac{E}{RT}\right) \quad (15)$$

Where, A is the pre-exponential factor (s^{-1}), E is the activation energy (kJ·mol^{-1}), and R is the gas constant (8.314 J·mol^{-1}·K^{-1}).

The activations of graphite and coke with oxidizing gas are a heterogeneous gas−solid reaction, in which pore structure and

dx.doi.org/10.1021/ie4039955 | Ind. Eng. Chem. Res. 2014, 53, 5737−5748

surface area of the solid particle are changing due to the reaction. These structural variations and other phenomena such as film mass transfer, pore diffusion, and chemical reaction caused by catalytic have to be considered.[24] Thus, many different mechanism functions were chosen in order to find the best one. The differential and integral expressions of common gas−solid reaction mechanism functions are shown in Table 4.[25−27]

Table 4. Function $f(x)$ of the Most Common Solid−Gas Reaction Models, Together with Integral Forms $F(x)$

symbol	reaction model	$f(x)$	$F(x) = \int_0^x \mathrm{d}x/f(x)$
A_1	nuclei production ($n = 1$)	$1 - x$	$-\ln(1 - x)$
A_2	Avrami−Erofeev ($n = 2$)	$2(1 - x)[-\ln(1 - x)]^{1/2}$	$[-\ln(1 - x)]^{1/2}$
C_1	phase boundary reaction ($n = 2$)	$(1 - x)^2$	$(1 - x)^{-1} - 1$
C_2	phase boundary reaction ($n = 3/2$)	$2(1 - x)^{3/2}$	$(1 - x)^{-1/2}$
D_1	dimensional diffusion	$1/2x$	x^2
D_2	two-dimensional diffusion	$[-\ln(1 - x)]^{-1}$	$x + (1 - x)\ln(1 - x)$
D_3	three-dimensional diffusion (Jander)	$(3/2)(1 - x)^{2/3}[1 - (1 - x)^{1/3}]^{-1}$	$[1 - (1 - x)^{1/3}]^2$
R_1	shrinking core model	$2(1 - x)^{1/2}$	$1 - (1 - x)^{1/2}$
R_2	shrinking core model	$3(1 - x)^{2/3}$	$1 - (1 - x)^{1/3}$
R_3	shrinking core model ($n = 2$)	$(1/2)(1 - x)^{-1}$	$1 - (1 - x)^2$

Inserting the mechanism function and eq 15 into eq 14, the mathematical description of the data from the reaction is usually defined in terms of a kinetic triplet $(E, A, f(x))$,[28] as shown below:

$$\frac{\mathrm{d}x}{\mathrm{d}t} = A \exp\left(-\frac{E}{RT}\right) f(x) \tag{16}$$

Under constant heating rate

$$\frac{\mathrm{d}T}{\mathrm{d}t} = \beta = \text{constant} \tag{17}$$

Thus, after substation in eq 16 with eq 17 and some transformations, the final kinetic equation can be expressed as below:

$$\frac{\mathrm{d}x}{f(x)} = \frac{A}{\beta} \exp\left(-\frac{E}{RT}\right) \mathrm{d}T \tag{18}$$

(2) Solving Methods. Traditionally, there are two classes of methods using nonisothermal data to determine the kinetic parameters used in eq 18.[29] One is the derivative method which simply requires a linearization of this equation after taking the natural log of both sides. Then, for a certain conversion (x) at a chosen heating rate, the natural logarithm of the conversion rate $(\ln(\mathrm{d}x/\mathrm{d}t))$ plotted against T^{-1} gives a straight line with the slope $(-E/R)$.[30] Therefore, E can be obtained by calculating the slope at different conversion values (x). The Freeman−Carroll and the Doyle are the most common derivative methods.[31] The integral method is the other common method for determining kinetic parameters from nonisothermal data. Coats−Redfern and Metzger are the common integral methods.[31] This paper adopted the Coats−Redfern method[32] to calculate the kinetic parameters. An integration function of eq 18 is shown as

$$\int_0^x \frac{\mathrm{d}x}{f(x)} = \int_{T_0}^{T_x} \frac{A}{\beta} \exp\left(-\frac{E}{RT}\right) \mathrm{d}T \tag{19}$$

Where, T_0 is the starting temperature of the reaction, and T_x is the temperature at conversion x. The right-hand side of eq 19 has no exact analytical solution, but by making some variable substitutions and applying Cauchy's rule, the expression can be solved, as shown below:

$$\int_{T_0}^{T_x} \frac{A}{\beta} \exp\left(-\frac{E}{RT}\right) \mathrm{d}T \cong \frac{ART_x^2}{\beta E}\left(1 - \frac{2RT_x}{E}\right)\exp\left(-\frac{E}{RT_x}\right) \tag{20}$$

The solution of the integral on the left-hand side of eq 19 is usually defined as below:

$$F(x) = \int_0^x \frac{\mathrm{d}x}{f(x)} \tag{21}$$

Then, after division by T^2 and taking logarithms, eq 19 is transferred to

$$\ln\left(\frac{F(x)}{T^2}\right) = \ln\left[\frac{AR}{\beta E}\left(1 - \frac{2RT}{E}\right)\right] - \frac{E}{RT} \tag{22}$$

Since $2RT/E \ll 1$, eq 22 can be approximated to be

$$\ln\left(\frac{F(x)}{T^2}\right) = \ln\frac{AR}{\beta E} - \frac{E}{RT} \tag{23}$$

The most probable mechanism function can be obtained by analyzing the linear relationship between $\ln[F(x)/T^2]$ and $1/T$ using different $F(x)$. The activation energy and frequency factor can be calculated using this mechanism function, as shown in Table 4. The equation of regression correlation coefficient is shown as follows.

$$r = \frac{\sum_{i=1}^{i=n}(x_i - \bar{x})(y_i - \bar{y})}{\sqrt{\sum_{i=1}^{i=n}(x_i - \bar{x})^2 (y_i - \bar{y})^2}} \tag{24}$$

Where, x_i and y_i are experimental points, and $\bar{x}$ and $\bar{y}$ are the average value of x_i and y_i, respectively.

4. RESULTS AND DISCUSSION

4.1. Gasification Process of Graphite and Coke. Figure 5 represents the process of weight loss of graphite gasification and coke gasification. A process of weight gain was observed before the weight loss in both graphite and coke gasification. Two stages were proposed to explain this reaction process in a recent study.[33] The initial stage was an exothermic slow gasification stage caused by the combined effect of the exothermic chemisorption and the endothermic chemical reaction.[33,34] And then the fast gasification stage began, while the chemisorption step stopped.[33] Although many mechanisms have been put forward to interpret carbon gasification process,[13,35,36] none have been accepted widely due to the difficulty of in situ observation of the evolution of molecules in the whole reaction process. However, the entire carbon gasification process can be monitored using thermogravimetry, which has been widely applied to study the kinetics of carbon gasification.[37−39] Even though graphite possessed a smaller

dx.doi.org/10.1021/ie4039955 | Ind. Eng. Chem. Res. 2014, 53, 5737−5748

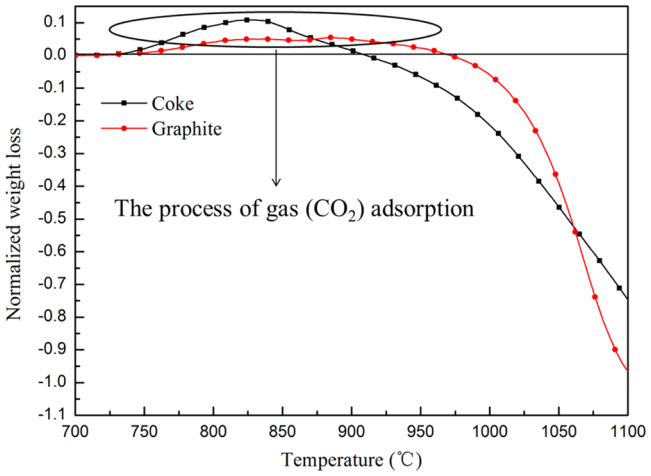

Figure 5. Difference of weight loss in the gasification reactions of graphite and coke.

particle size and greater surface area than that of coke (Figure 1), CO_2 reacted with coke at a lower temperature than it did with graphite (Figure 5). This may be caused by two factors: (i) the structure of coke carbon is different from that of graphite carbon; (ii) the minerals in coke had a catalytic effect on the coke gasification. Both reasons will be further confirmed below.

4.2. Effect of Alkali Carbonates on Graphite Gasification. Considering the fluctuation of reaction in the initial stage was unavoidable due to the gas adsorption as discussed before, the gasification curve while the conversion was greater than 0.05 and less than 1.00 was intercepted to compare the entire gasification procedure of graphite gasification and coke gasification under the influence of Na_2CO_3 or K_2CO_3. Thus the temperatures at carbon conversion 0.05 and 1.00 were set as the initial reaction temperature (T_0) and the final reaction temperature (T_f), respectively, in this paper. The derivative of the carbon conversion curve was calculated and normalized to obtain the fluctuation of reaction rate and find the T_{max}. T_0, T_f, and T_{max} were defined as the characteristic temperatures of the gasification reaction procedure.

Figures 6 and 7 show the carbon conversion and normalized reaction rate versus temperature in graphite gasification with different contents of Na_2CO_3 or K_2CO_3 at constant heating rate. It can be observed that, with increasing Na_2CO_3 content, the carbon conversion curve shifts to a lower temperature zone. At the same reaction temperature, the higher the Na_2CO_3 or K_2CO_3 content, the higher the carbon conversion is. However, the catalytic effect of both Na_2CO_3 and K_2CO_3 seems to reach a limitation when their contents are higher than 2.5%, because the carbon conversion curve at 2.5% and 5.0% catalytic is nearly overlapped with each other and higher catalytic content cannot shift the carbon conversion curve any more.

The characteristic temperatures of graphite gasification, as defined before, were obtained from Figures 6 and 7. The characteristic temperatures were plotted versus the content of catalytic, and the results are shown in Figure 8. This indicates clearly that T_0, T_{max}, and T_f decrease obviously when the content of catalytic is below 2.5% and then reach a limitation when the content of catalytic is above 2.5%. It can also be observed that the influence of Na_2CO_3 and K_2CO_3 on graphite gasification are similar with each other. However, the catalytic effect of simple substance vapors of K was confirmed to be greater than that of Na in previous study.[11] Thus, the catalytic

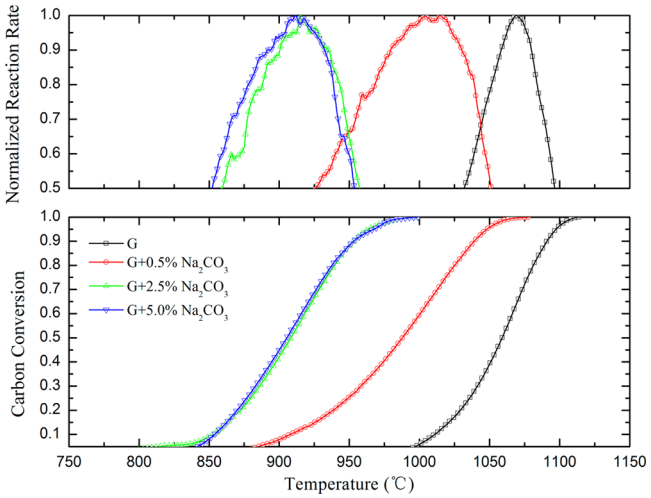

Figure 6. Carbon conversion and normalized reaction rate versus temperature in graphite gasification with different content of Na_2CO_3 at constant heating rate (5 K/min).

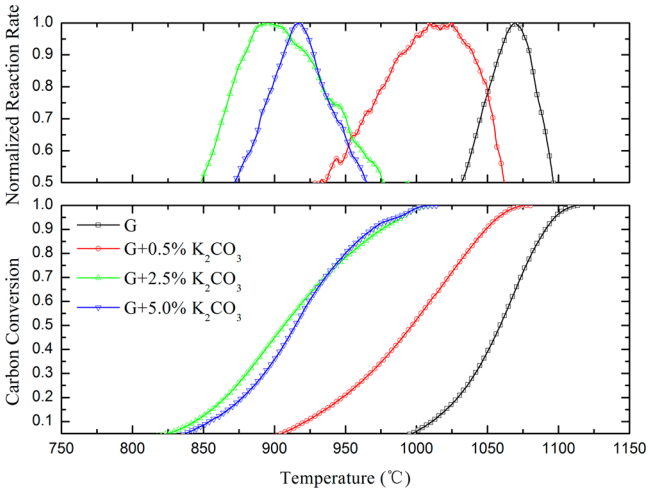

Figure 7. Carbon conversion and normalized reaction rate versus temperature in graphite gasification with different content of K_2CO_3 at constant heating rate (5 K/min).

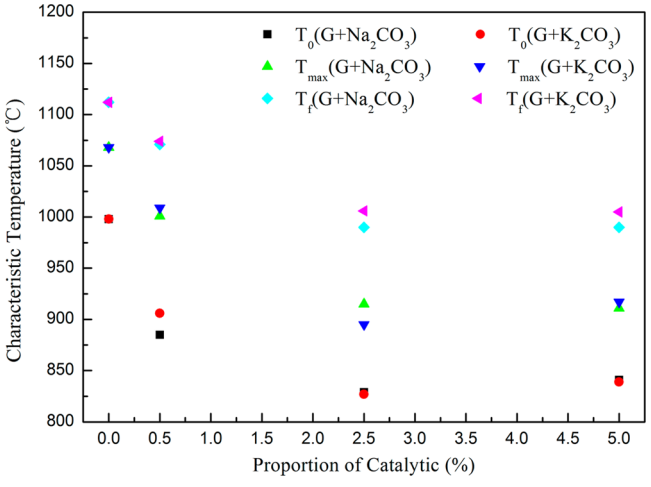

Figure 8. Influence of Na_2CO_3 and K_2CO_3 on the characteristic temperatures of graphite gasification.

dx.doi.org/10.1021/ie4039955 | Ind. Eng. Chem. Res. 2014, 53, 5737−5748

mechanism of alkali carbonates and vapors must be different, which needs further study.

4.3. Effect of Alkali Carbonates on Coke Gasification. The carbon conversion and normalized reaction rate versus temperature in coke gasification with different contents of catalyst (N_2CO_3 and K_2CO_3) are shown in Figures 9 and 10.

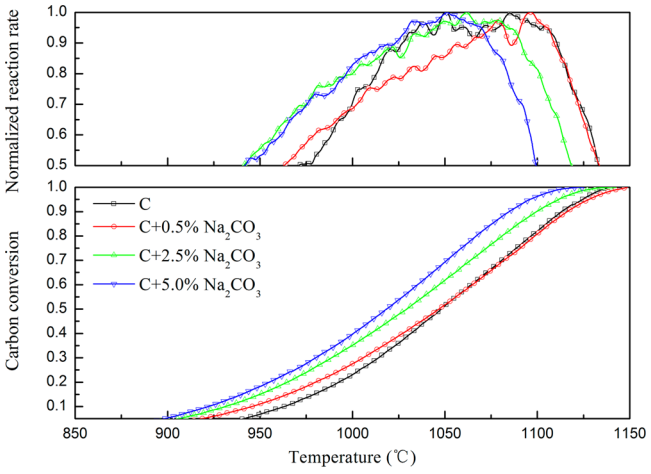

Figure 9. Carbon conversion and normalized reaction rate versus temperature in coke gasification with different content of Na_2CO_3 at constant heating rate (5 K/min).

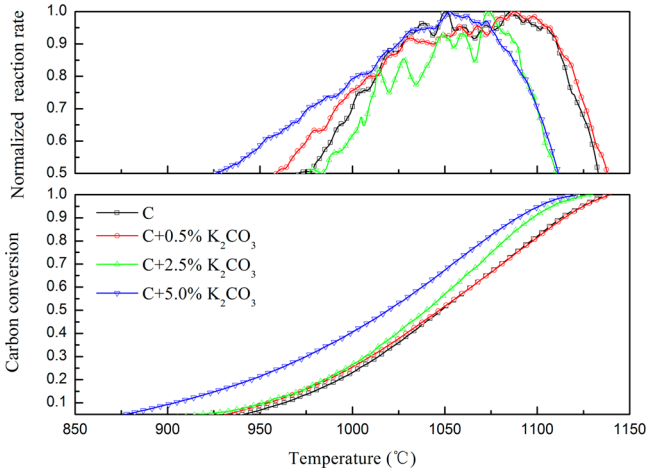

Figure 10. Carbon conversion and normalized reaction rate versus temperature in coke gasification with different content of K_2CO_3 at constant heating rate (5 K/min).

The trend of the catalytic effect on coke gasification is similar with that on graphite gasification. However, compared with the influence of catalyst on graphite gasification, the alkali carbonate has smaller influence on the coke gasification process. The carbon conversion curves are almost in the same position while the proportion of alkali carbonates are 0.0% and 0.5%. The gap between the conversion curve of coke gasification at 2.5% and 5.0% alkali carbonates is also not as clear as that of graphite gasification.

Using the same method to obtain the characteristic temperatures of the gasification process as mentioned in section 4.1, T_0, T_{max}, and T_f of coke gasification were obtained from Figures 9 and 10. The characteristic temperatures of coke gasification were plotted versus the content of catalyst, and the results are shown in Figure 11. It can be observed that Na_2CO_3

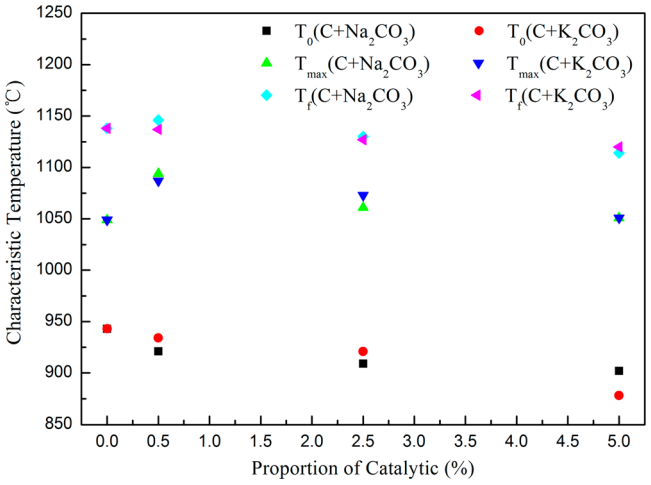

Figure 11. Influence of catalyst on the characteristic temperatures of coke gasification.

and K_2CO_3 have a similar small influence on the coke gasification with CO_2, which indicates that the catalytic effects of Na_2CO_3 and K_2CO_3 on the coke gasification are too weak to lower the reaction barrier. The cause of this phenomenon will be discussed below.

4.4. Comparison of Graphite Gasification and Coke Gasification. The initial temperature of carbon gasification is the most important one among the characteristic temperatures because it determines the boundary between direct reduction and indirect reduction in the blast furnace.[4] Figure 12 shows

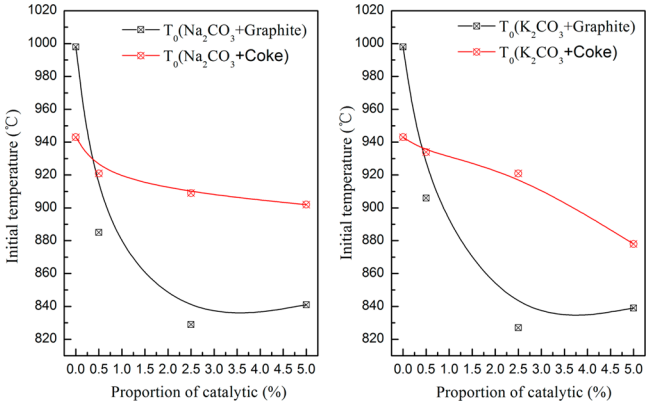

Figure 12. Different influence of Na_2CO_3 and K_2CO_3 on the initial temperature of graphite and coke gasification reactions.

the difference of initial reaction temperatures in this study. It indicates that the influence of Na_2CO_3 and K_2CO_3 on the graphite gasification is obvious, while the coke gasification can only be slightly affected by addition Na_2CO_3 and K_2CO_3. The degree of catalytic effect of Na_2CO_3 and K_2CO_3 on graphite gasification and coke gasification are similar with each other.

5. STUDY OF CATALYTIC MECHANISM MODEL

5.1. Determine the Most Probable Mechanism Function. It has been confirmed that the kinetic parameters calculated with different methods strongly depend on the selection of proper mechanism function.[40] Therefore, it is very important to determine the most probable mechanism function. On the basis of the kinetic analysis and calculation procedures

dx.doi.org/10.1021/ie4039955 | Ind. Eng. Chem. Res. 2014, 53, 5737−5748

Table 5. Correlation Coefficient Calculated Using Different Mechanism Functions

sym	A_1	A_2	C_1	C_2	D_1	D_2	D_3	R_1	R_2	R_3	max r	best model
G	0.9992	0.9993	0.9551	0.8553	0.8553	0.9885	0.9976	0.9945	0.9977	0.9517	0.9993	A_2
G-N1	0.9983	0.9985	0.9544	0.8595	0.8595	0.9931	0.9992	0.9974	0.9993	0.9643	0.9993	R_2
G-N2	0.9989	0.9991	0.9710	0.8884	0.8884	0.9800	0.9927	0.9884	0.9932	0.9423	0.9991	A_2
G-N3	0.9946	0.9953	0.9838	0.9222	0.9222	0.9643	0.9830	0.9769	0.9841	0.9115	0.9953	A_2
G-K1	0.9976	0.9978	0.9564	0.8616	0.8616	0.9904	0.9974	0.9954	0.9976	0.9572	0.9978	A_2
G-K2	0.9942	0.9950	0.9796	0.9110	0.9110	0.9710	0.9855	0.9812	0.9867	0.9282	0.9950	A_2
G-K3	0.9967	0.9971	0.9829	0.9183	0.9183	0.9747	0.9884	0.9841	0.9893	0.9348	0.9971	A_2
C	0.9978	0.9981	0.9669	0.8783	0.9824	0.9900	0.9967	0.9948	0.9970	0.9592	0.9981	A_2
C-N1	0.9986	0.9989	0.9998	0.9877	0.9959	0.9969	0.9978	0.9976	0.9980	0.9927	0.9998	R_2
C-N2	0.9982	0.9985	0.9672	0.8850	0.9844	0.9916	0.9977	0.9960	0.9980	0.9625	0.9985	A_2
C-N3	0.9982	0.9984	0.9663	0.8842	0.9864	0.9931	0.9984	0.9970	0.9986	0.9654	0.9986	R_2
C-K1	0.9980	0.9982	0.9702	0.8863	0.9853	0.9919	0.9974	0.9959	0.9977	0.9639	0.9982	A_2
C-K2	0.9982	0.9984	0.9578	0.8580	0.9893	0.9950	0.9995	0.9983	0.9996	0.9706	0.9996	R_2
C-K3	0.9985	0.9988	0.9994	0.9875	0.9958	0.9968	0.9976	0.9975	0.9979	0.9927	0.9994	C_1

introduced in section 3.2, the correlation coefficient (r) was calculated. The coefficient varied greatly when different mechanism functions were chosen. With each mechanism function in Table 4, the corresponding correlation coefficient for each conversion curve, shown in Figures 6, 7, 9, and 10 was calculated. The results are presented in Table 5. The higher the correlation coefficient, the better the corresponding mechanism can describe the kinetic curve. As shown in Table 5, the best mechanism function for both graphite and coke gasification is the A_2 model. With adding alkali carbonates in the samples, the R_2 model also shows a good description of the kinetic curve in some cases such as (G + N1), (C + N1), (C + N3), (C + K2). Some individual cases such as (C + K3) can be described with the C_1 model. Generally, A_2 can guarantee the correlation coefficient greater than 0.99 in all cases, thus it was determined to be the most probable mechanism function in this study.

The most probable mechanism function is expressed as below.

$$f(x) = 2(1 - x)[-\ln(1 - x)]^{1/2} \quad (25)$$

This model originally belonged to a combined form of mechanism function suggested for the preliminary appraisal of possible mechanism.[41] It is expressed as below.

$$f(x) = x^m(1 - x)^n[-\ln(1 - x)]^p \quad (26)$$

Where, m, n, and p are empirically obtained exponent factors, and one of them is always zero.[41] The combinations of different values of m, n, and p make it possible to describe various probable mechanisms.[40,41] In this study, m was zero, n was 1, and p was 0.5. This combination indicated the most probable mechanism of the rate-controlled stages are two- and three-dimensional growing of nuclei (Avrami−Erofeev equation) and acceleratory or deceleratory rate of nuclei growth.[41] However, this appraisal cannot give the direct answer in the search for a true reaction mechanism. The overlapping of the values of the exponent factors, as well as the expected difficulties with the numerical solution of eq 26, will only provide a rough idea of the possible reaction mechanisms. Thus, a complementary direct investigation of the process by means of X-ray diffraction and/or microscopy becomes necessary.

5.2. Calculation of Kinetic Parameters. Using the methods introduced in section 3.2, the kinetic parameters were calculated and the results are shown in Table 6. The activation energy was plotted versus the proportion of alkalis added to illustrate the influence of alkali carbonated, as shown in Figure 13. It is observed that the activation energy of graphite, which is the highest among all samples, can be reduced by adding alkali carbonates, which exist as catalyst. However, the activation energy of coke cannot be reduced by adding alkali carbonates because it is originally low and nearly the lowest level of activation energy of graphite. This indicates that coke carbon has been activated to a lower level by its inner factors.

Table 6. Kinetic Parameters Calculated by Simulated Annealing

samples	ln(A) (s^{-1})	E (kJ/mol)	samples	ln(A) (s^{-1})	E (kJ/mol)
graphite	54.3073	309.5687	coke	41.196	169.9946
G + 0.5% Na_2CO_3	42.6324	177.4101	C + 0.5% Na_2CO_3	39.3331	150.3264
G + 2.5% Na_2CO_3	45.0177	190.8864	C + 2.5% Na_2CO_3	39.3507	149.0763
G + 5.0% Na_2CO_3	44.9182	189.8683	C + 5.0% Na_2CO_3	39.6243	150.7648
G + 0.5% K_2CO_3	43.2525	184.8151	C + 0.5% K_2CO_3	40.2254	159.7755
G + 2.5% K_2CO_3	41.1449	155.2310	C + 2.5% K_2CO_3	41.4668	171.5405
G + 5.0% K_2CO_3	43.0722	173.8239	C + 5.0% K_2CO_3	37.1967	126.7206

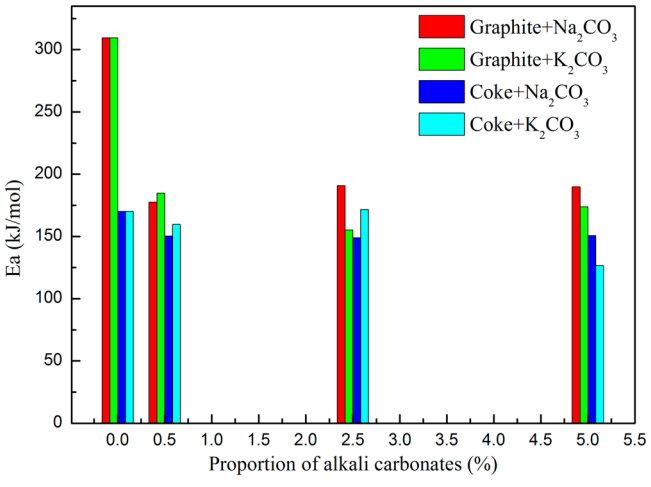

Figure 13. Change of activation energy with the addition of catalyst.

dx.doi.org/10.1021/ie4039955 | Ind. Eng. Chem. Res. 2014, 53, 5737−5748

Figure 14 shows the relationship between activation energy and pre-exponential factor. It can be observed that the

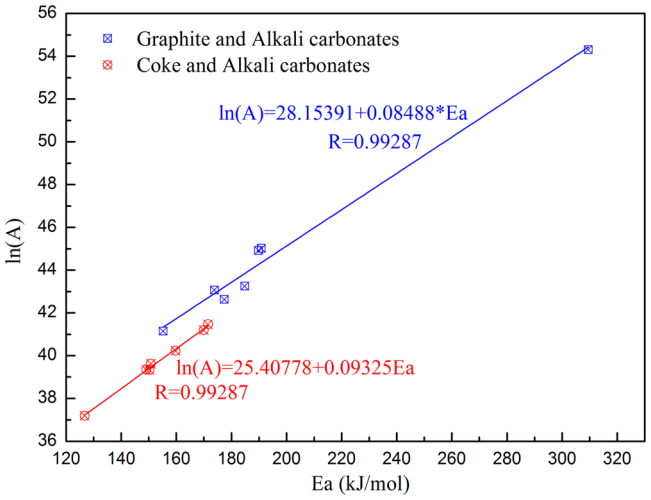

Figure 14. Kinetic compensation of activation energy and pre-exponential factor (graphite and coke).

frequency factor is linearly related to the activation energy. This indicates that the kinetic compensation effect exists in both graphite gasification and coke gasification under the influence of alkali carbonates. For instance, the kinetic compensation effect of graphite/CO_2 reaction with alkali carbonates is shown in eq 27 and that of coke/CO_2 reaction with alkali is shown as eq 28.

$$\ln(A) = 28.15391 + 0.08488E_a \quad (27)$$

$$\ln(A) = 25.40778 + 0.09325E_a \quad (28)$$

5.3. Kinetic Model of Gasification Catalyzed by Alkali Carbonates. The kinetic model of both graphite and coke gasification with CO_2 under the influence of alkali carbonates can be obtained, using the most probable mechanism function, the activation energy, and frequency factor which were obtained before. For example, the kinetic models of graphite and coke without adding alkali carbonates could be expressed as eqs 29 and 30, respectively.

$$\frac{dx}{dt} = 7.6982 \times 10^{23}\exp\left(-\frac{309.5687}{RT}\right)(1-x)[-\ln(1-x)]^{1/2} \quad (29)$$

$$\frac{dx}{dt} = 1.5568 \times 10^{18}\exp\left(-\frac{169.9946}{RT}\right)(1-x)[-\ln(1-x)]^{1/2} \quad (30)$$

5.4. Causes for the Difference Between Graphite Gasification and Coke Gasification. The kinetic analysis combined with the thermogravimetric experimental results revealed the apparent difference between graphite gasification and coke gasification with CO_2. However, the reactivity of carbon is closely related with its structure,[42,43] and the key distinction between graphite and coke should be investigated with direct detection. Thus, X-ray diffraction and Raman spectroscopy techniques were used to characterize the different inner structures of graphite and coke. Figure 15 represents the X-ray diffraction pattern of graphite and coke. The coke

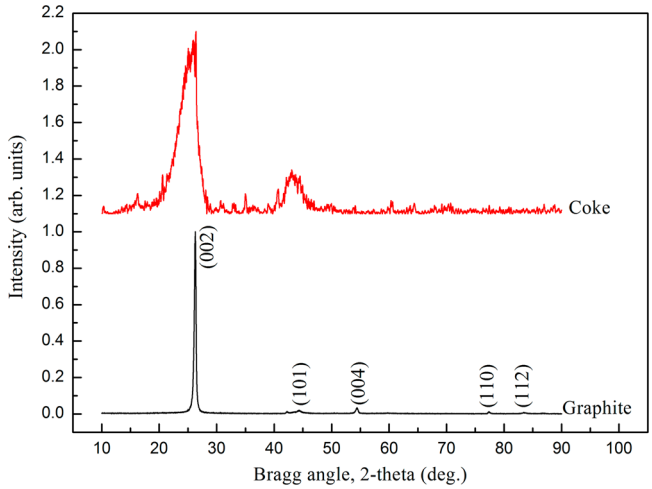

Figure 15. X-ray diffraction patterns of graphite and coke.

represents a wider main peak than graphite in the X-ray diffraction pattern, which is caused by its highly disordered and heterogeneous structure. The X-ray diffraction pattern can only represent the average unit-cell or crystallite. As the crystallinity decreases, the structure of coke cannot be obtained by X-ray diffraction. However, the Raman spectrum is a good method to characterize the different structure of carbon.

Figure 16 shows the Raman spectra of the graphite and coke samples. It can be observed that the graphite sample possesses

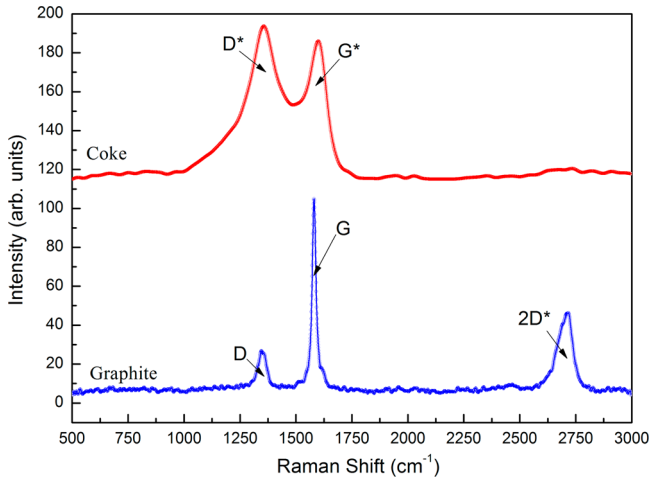

Figure 16. Raman spectra of graphite and coke in this experiment.

an ordered structure and has an obviously separate G band (graphite E_{2g}^2 mode with D_{6h}^4 crystal symmetry) and D band (reflecting the disordered structure or in-plane defects located between the basic structural units (BSUs)). However, the interpretation of the Raman spectral data for coke differs distinctly from that for the highly condensed/graphitized carbon materials, due to its highly disordered and heterogeneous structure. Quantitative correlation between Raman spectra and structural parameters may not be achieved by simply considering the D peak/band and the G peak/band,[44−48] mainly due to the large "overlap" between these two "bands" for coke. In fact, much more structure is hidden in the overlap between the G and D bands for highly disordered carbonaceous material.

dx.doi.org/10.1021/ie4039955 | Ind. Eng. Chem. Res. 2014, 53, 5737−5748

The FT-Raman spectra of coke in this study over the range of 900−1900 cm^{-1} were curve-fitted with the combination of three Lorentzian bands (G, G_R, and D_L) and three Gaussian bands (G_R, D, and D_L), as shown in Figure 17. In order to

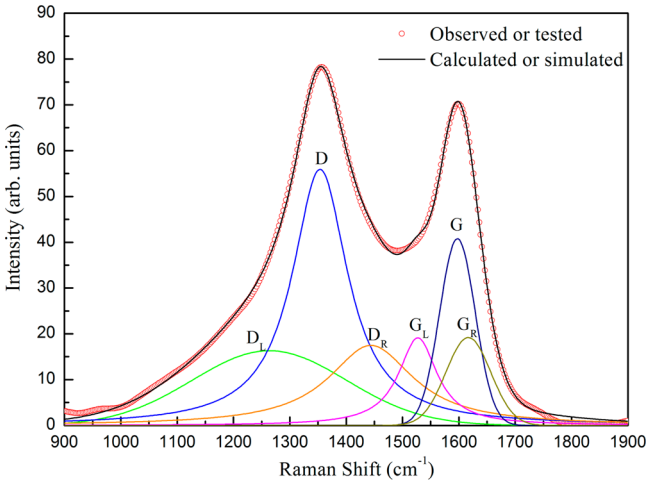

Figure 17. Curve-fitting of the Raman spectrum of coke with six peaks.

reproduce the experimentally obtained spectrum, it was necessary to assume additional peaks of D_L, D_R, G_L, and G_R. The D_L and D_R peaks appeared near 1263 and 1443 cm^{-1}, respectively. The G_L and G_R peaks appeared near 1527 and 1616 cm^{-1}, respectively. These additional peaks were assigned to the so-called turbostratic or random structure in the coke.[16,49] The overall Raman intensity (peak area) as well as the ratios among the intensities of some major Raman bands has allowed some semiquantitative evaluation of difference between graphite structure and coke structure. The ratio (A_i/A_t) between the area of *i* band and the total areal of all bands has been extensively used as an important parameter to study the crystalline or graphite-like carbon structure.[16,48,50] The ratios of each band area in the total area were calculated and compared in this study. The results are shown in Figure 18. It is

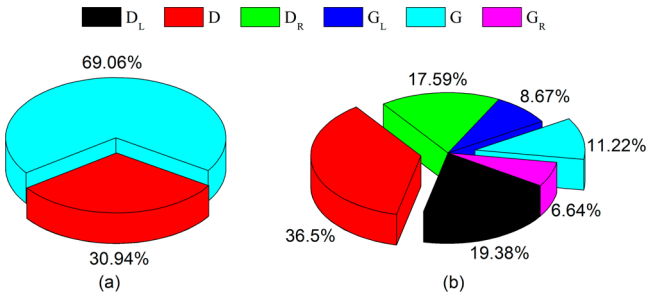

Figure 18. Ratios of the area of different bands in the total bands area (a) graphite and (b) coke.

clear that ratio of G bands of graphite (69.06%) is much greater than that of coke (11.22%), which indicates graphite structure is more ordered than coke structure and small part of graphite-like structure exists in coke structure. Combined with the analysis in section 5.2, it seems that graphite-like structure has higher activation energy and random structure in coke is easier to react with CO_2.

6. CONCLUSIONS

(1) The thermodynamics of possible reactions in the C−CO_2−Na_2CO_3/K_2CO_3 system was calculated by FactSage. The results showed that, at the same temperature, the higher the pressure, the lower the fraction of CO. The fraction curve of CO shifted to higher temperature zone with increasing pressure, which indicated that high pressure made it harder for the carbon gasification to occur. There was a cross point between the fraction curve of CO and that of CO_2. The lower the cross temperature, the easier the carbon gasification. With increasing pressure, the cross temperature increased. Further study was needed to study the influence of pressure on the reactions in the C−CO_2−Na_2CO_3/K_2CO_3 system.

(2) The nonisothermal method was adopted to get the mass (or conversion) versus temperature curve under a controlled heating rate using TGA. A process of gas adsorption was observed before the gasification process. This process would cause a fluctuation of reaction rate in the initial stage of reaction. The alkali carbonates (Na_2CO_3/K_2CO_3) had a catalytic effect on the gasification reactions of both graphite and coke. Graphite was tested to be more vulnerable to be catalyzed by alkali carbonates. However, there was a limitation for the catalytic effect. To graphite, 5% seemed to be the maximum proportion of alkali carbonates to cause a catalytic effect. To blast furnace coke, the limitation was much lower, due to its highly disordered carbon structure and the influence of both original and exotic alkali carbonates.

(3) Ten kinetic models were adopted and calculated to determine the most probable mechanism function of graphite gasification and coke gasification. It was found that the experimental data were best described by the Avrami−Erofeev equation for two- and three-dimension growing of nuclei-controlled reactions. The values of activation energy and frequency factor were calculated with the best probable kinetic equation. The compensation effect was confirmed to exist between activation energy and pre-exponential factor in both graphite gasification and coke gasification. The activation energy of coke could not be reduced by adding Na_2CO_3/K_2CO_3 because it was originally low and nearly the lowest level of activation energy of graphite. This indicated that carbon in coke had been activated to the lowest level by its inner factors.

(4) X-ray diffraction and Raman spectroscopy techniques were used to characterize the different inner structures of graphite and coke. Graphite showed a highly ordered structure, while it was difficult to characterize the structure of coke as to its highly disordered and heterogeneous structure. The Raman spectra of graphite consisted of two separate peaks of G and D, while that of coke consists of two overlap peaks of G* and D*. These peaks of coke could be simulated by six peaks of G_L, G, G_R, D_L, D, and D_R. The area ratios of different bands indicated graphite structure was more ordered than coke structure and a small part of graphite-like structure existed in coke structure. Graphite-like structure had higher activation energy and random structure in coke was easier to react with CO_2

dx.doi.org/10.1021/ie4039955 | Ind. Eng. Chem. Res. 2014, 53, 5737−5748

AUTHOR INFORMATION

Corresponding Author

*E-mail: zhang.jianliang@hotmail.com. Phone: +86-10-62332364; +86-13910019986. Mailing address: No. 30 Xueyuan Rd, Haidian District, Beijing, 100083, China.

Notes

The authors declare no competing financial interest.

ACKNOWLEDGMENTS

This work was financially supported by the National Basic Research Program of China (2012CB720401), the National Natural Science Foundation of China, and Baosteel Group Co., LTD, of Shanghai for the Key Joint Project (U1260202) and the Postdoctoral Science Foundation of China (No. 2012T50045). The authors thank Baosteel for providing samples and an opportunity to undertake this research.

REFERENCES

(1) Li, K.; Zhang, J.; Zhang, Y.; Liu, Z.; Jiang, X. Critical analyses about the development of iron-making process based on the principle of energy-saving and emission reduction. *Chinese J. Proc. Eng.* **2014**, *14*, 162−172.

(2) Liu, Z.; Zhang, J.; Zuo, H.; Yang, T. Recent Progress on Long Service Life Design of Chinese Blast Furnace Hearth. *ISIJ Int.* **2012**, *52*, 1713−1723.

(3) Li, R. Analysis of Carbon Reduction Wasy in China's Ironmaking System. *China Metall.* **2012**, *22*, 40−46.

(4) Zhang, J.; Zhang, X.; Guo, H.; Chang, J.; Zuo, H.; Guo, H. Study on the test methods of coke reactivity index and starting temperature of coke solution loss reaction. *Ironmaking* **2011**, *30*, 27−29.

(5) Grigore, M.; Sakurovs, R.; French, D.; Sahajwalla, V. Influence of mineral matter on coke reactivity with carbon dioxide. *ISIJ Int.* **2006**, *46*, 503−512.

(6) Gornostayev, S. S.; Härkki, J. J. Graphite crystals in blast furnace coke. *Carbon* **2007**, *45*, 1145−1151.

(7) Kawakami, M.; Taga, H.; Takenaka, T.; Yokoyama, S. Micro pore structure and reaction rate of coke, wood charcoal and graphite with CO_2. *ISIJ Int.* **2004**, *44*, 2018−2022.

(8) Kubota, Y.; Nomura, S.; Arima, T.; Kato, K. Quantitative Evaluation of Relationship between Coke Strength and Pore Structure. *ISIJ Int.* **2011**, *51*, 1800−1808.

(9) Yang, J. *Catalytic effect and mechanism of minerals on the gasification reaction of blast furnace coke*. Ph.D. Thesis, Dongbei University, Shenyang, 2000.

(10) Gupta, S.; Ye, Z.; Kim, B.-c.; Kerkkonen, O.; Kanniala, R.; Sahajwalla, V. Mineralogy and reactivity of cokes in a working blast furnace. *Fuel Process. Technol.* **2013**, *117*, 30−37.

(11) Zhao, H.; Cheng, S. New cognition on coke degradation by potassium and sodium in alkali enriched regions and quantificational control model for BF. *J. Univ. Sci. Technol. Beijing* **2012**, *34*, 333−341.

(12) Zhang, Q. Accumulation and circulation of alkalis in the BF. *Iron Steel* **1982**, *17*, 75−77.

(13) Chen, S. G.; Yang, R. T.; Kapteijn, F.; Moulijn, J. A. A new surface oxygen complex on carbon: toward a unified mechanism for carbon gasification reactions. *Ind. Eng. Chem. Res.* **1993**, *32*, 2835−2840.

(14) Lee, W. J.; Kim, S. D. Catalytic activity of alkali and transition metal salt mixtures for steam-char gasification. *Fuel* **1995**, *74*, 1387−1393.

(15) Chen, S. G.; Yang, R. T. Unified Mechanism of Alkali and Alkaline Earth Catalyzed Gasification Reactions of Carbon by CO_2 and H_2O. *Energy Fuel* **1997**, *11*, 421−427.

(16) Kawakami, M.; Karato, T.; Takenaka, T.; Yokoyama, S. Structure analysis of coke, wood charcoal and bamboo charcoal by Raman spectroscopy and their reaction rate with CO_2. *ISIJ Int.* **2005**, *45*, 1027−1034.

(17) Gupta, S.; Ye, Z.; Kanniala, R.; Kerkkonen, O.; Sahajwalla, V. Coke graphitization and degradation across the tuyere regions in a blast furnace. *Fuel* **2013**, *113*, 77−85.

(18) Gupta, S.; French, D.; Sakurovs, R.; Grigore, M.; Sun, H.; Cham, T.; Hilding, T.; Hallin, M.; Lindblom, B.; Sahajwalla, V. Minerals and iron-making reactions in blast furnaces. *Prog. Energ. Combust.* **2008**, *34*, 155−197.

(19) Zhang, S. *Materials Characterization Techniques*; Science Press: Beijing, 2010.

(20) Shao, J.; Yan, R.; Chen, H.; Wang, B.; Lee, D. H.; Liang, D. T. Pyrolysis Characteristics and Kinetics of Sewage Sludge by Thermogravimetry Fourier Transform Infrared Analysis. *Energy Fuels* **2007**, *22*, 38−45.

(21) Li, S.; Yue, C. Study of pyrolysis kinetics of oil shale. *Fuel* **2003**, *82*, 337−342.

(22) Burnham, A. K.; Braun, R. L. Global kinetic analysis of complex materials. *Energy Fuels* **1999**, *13*, 1−22.

(23) Molina, A.; Mondragón, F. Reactivity of coal gasification with steam and CO_2. *Fuel* **1998**, *77*, 1831−1839.

(24) Moulijn, J. A.; Cerfontain, M.; Kapteijn, F. Mechanism of the potassium catalysed gasification of carbon in CO_2. *Fuel* **1984**, *63*, 1043−1047.

(25) Tanaka, H. Thermal analysis and kinetics of solid state reactions. *Thermochim. Acta* **1995**, *267*, 29−44.

(26) Vlaev, L.; Markovska, I.; Lyubchev, L. Non-isothermal kinetics of pyrolysis of rice husk. *Thermochim. Acta* **2003**, *406*, 1−7.

(27) Li, P.; Yu, Q.; Qin, Q.; Lei, W. Kinetics of CO_2/Coal Gasification in Molten Blast Furnace Slag. *Ind. Eng. Chem. Res.* **2012**, *51*, 15872−15883.

(28) Vyazovkin, S. Model-free kinetics. *J. Therm. Anal. Calorim.* **2006**, *83*, 45−51.

(29) Popescu, C.; Segal, E. Critical considerations on the methods for evaluating kinetic parameters from nonisothermal experiments. *Int. J. Chem. Kinet.* **1998**, *30*, 313−327.

(30) Zhang, X.; de Jong, W.; Preto, F. Estimating kinetic parameters in TGA using B-spline smoothing and the Friedman method. *Biomass Bioenerg.* **2009**, *33*, 1435−1441.

(31) Wendlandt, W. W. *Thermal methods of analysis*; Wiley-Interscience: New York, 1974.

(32) Coats, A.; Redfern, J. Kinetic parameters from thermogravimetric data. *Nature* **1964**, *201*, 68−69.

(33) Liu, Z.-S.; Wang, Q.; Zou, Z.-S.; Tan, G.-L. Reaction mechanism of carbon gasification in CO_2 under non-isothermal conditions. *J. Therm. Anal. Calorim.* **2011**, *104*, 1091−1096.

(34) Ergun, S. Kinetics of the reaction of carbon with carbon dioxide. *J. Phys. Chem.* **1956**, *60*, 480−485.

(35) Lizzio, A.; Piotrowski, A.; Radovic, L. Effect of oxygen chemisorption on char gasification reactivity profiles obtained by thermogravimetric analysis. *Fuel* **1988**, *67*, 1691−1695.

(36) Feng, B.; Bhatia, S. K. On the validity of thermogravimetric determination of carbon gasification kinetics. *Chem. Eng. Sci.* **2002**, *57*, 2907−2920.

(37) Barkia, H.; Belkbir, L.; Jayaweera, S. Non-isothermal kinetics of gasification by CO_2 of residual carbon from timahdit and tarfaya oil shale kerogens. *J. Therm. Anal. Calorim.* **2004**, *76*, 623−632.

(38) Amaya, A.; Píriz, J.; Tancredi, N.; Cordero, T. Activated carbon pellets from eucalyptus char and tar TG studies. *J. Therm. Anal. Calorim.* **2007**, *89*, 987−991.

(39) Fermoso, J.; Arias, B.; Pevida, C.; Plaza, M.; Rubiera, F.; Pis, J. Kinetic models comparison for steam gasification of different nature fuel chars. *J. Therm. Anal. Calorim.* **2008**, *91*, 779−786.

(40) Vlaev, L.; Nedelchev, N.; Gyurova, K.; Zagorcheva, M. A comparative study of non-isothermal kinetics of decomposition of calcium oxalate monohydrate. *J. Anal. Appl. Pyrol.* **2008**, *81*, 253−262.

(41) Šesták, J.; Berggren, G. Study of the kinetics of the mechanism of solid-state reactions at increasing temperatures. *Thermochim. Acta* **1971**, *3*, 1−12.

(42) Pusz, S.; Krzesińska, M.; Smędowski, Ł.; Majewska, J.; Pilawa, B.; Kwiecińska, B. Changes in a coke structure due to reaction with carbon dioxide. *Int. J. Coal Geol.* **2010**, *81*, 287−292.
(43) Grigore, M.; Sakurovs, R.; French, D.; Sahajwalla, V. Properties and CO_2 reactivity of the inert and reactive maceral-derived components in cokes. *Int. J. Coal Geol.* **2012**, *98*, 1−9.
(44) Johnson, C. A.; Patrick, J. W.; Mark Thomas, K. Characterization of coal chars by Raman spectroscopy, X-ray diffraction and reflectance measurements. *Fuel* **1986**, *65*, 1284−1290.
(45) Van Doorn, J.; Vuurman, M.; Tromp, P.; Stufkens, D.; Moulijn, J. Correlation between Raman spectroscopic data and the temperature-programmed oxidation reactivity of coals and carbons. *Fuel Process. Technol.* **1990**, *24*, 407−413.
(46) Schwan, J.; Ulrich, S.; Batori, V.; Ehrhardt, H.; Silva, S. Raman spectroscopy on amorphous carbon films. *J. Appl. Phys.* **1996**, *80*, 440.
(47) Cuesta, A.; Dhamelincourt, P.; Laureyns, J.; Martinez-Alonso, A.; Tascón, J. M. Comparative performance of X-ray diffraction and Raman microprobe techniques for the study of carbon materials. *J. Mater. Chem.* **1998**, *8*, 2875−2879.
(48) Potgieter-Vermaak, S.; Maledi, N.; Wagner, N.; Van Heerden, J.; Van Grieken, R.; Potgieter, J. Raman spectroscopy for the analysis of coal: a review. *J. Raman Spectrosc.* **2011**, *42*, 123−129.
(49) Lu, L.; Sahajwalla, V.; Kong, C.; Harris, D. Quantitative X-ray diffraction analysis and its application to various coals. *Carbon* **2001**, *39*, 1821−1833.
(50) Li, X.; Hayashi, J.i.; Li, C. Z. FT-Raman spectroscopic study of the evolution of char structure during the pyrolysis of a Victorian brown coal. *Fuel* **2006**, *85*, 1700−1707.